

Multi-band infrared CO₂ absorption sensor for sensitive temperature and species measurements in high-temperature gases

R. M. Spearrin · W. Ren · J. B. Jeffries ·
R. K. Hanson

Received: 29 October 2013 / Accepted: 17 January 2014
© Springer-Verlag Berlin Heidelberg 2014

Abstract A continuous-wave laser absorption diagnostic, based on the infrared CO₂ bands near 4.2 and 2.7 μm, was developed for sensitive temperature and concentration measurements in high-temperature gas systems using fixed-wavelength methods. Transitions in the respective R-branches of both the fundamental ν_3 band ($\sim 2,350\text{ cm}^{-1}$) and combination $\nu_1 + \nu_3$ band ($\sim 3,610\text{ cm}^{-1}$) were chosen based on absorption line-strength, spectral isolation, and temperature sensitivity. The R(76) line near $2,390.52\text{ cm}^{-1}$ was selected for sensitive CO₂ concentration measurements, and a detection limit of $<5\text{ ppm}$ was achieved in shock tube kinetics experiments ($\sim 1,300\text{ K}$). A cross-band, two-line thermometry technique was also established utilizing the R(96) line near $2,395.14\text{ cm}^{-1}$, paired with the R(28) line near $3,633.08\text{ cm}^{-1}$. This combination yields high temperature sensitivity ($\Delta E'' = 3,305\text{ cm}^{-1}$) and expanded range compared with previous intra-band CO₂ sensors. Thermometry performance was validated in a shock tube over a range of temperatures (600–1,800 K) important for combustion. Measured temperature accuracy was demonstrated to be better than 1 % over the entire range of conditions, with a standard error of $\sim 0.5\%$ and μs temporal resolution.

1 Introduction

High-temperature gas systems are ubiquitous in modern power, propulsion, and industrial processes. Accurate and

precise determination of temperature in such systems can be critical to understanding performance. Additionally, the determination of species concentration in high-temperature reacting gas flows provides a basis for characterizing reaction pathways and chemical kinetic mechanisms. Laser absorption diagnostics have been utilized extensively to measure gas temperature and species concentration in various high-temperature gas systems in both laboratory and industrial settings [1–3]. Non-intrusive, continuous-wave (CW) laser sensors provide the capability necessary for resolving the short time scales involved in chemistry and high-speed flow fields. This work presents a flexible, highly sensitive temperature and CO₂ concentration sensor based on mid-infrared absorption using two CW lasers, aimed at high-temperature gas environments.

Carbon dioxide (CO₂) is a major product of hydrocarbon combustion, a component in ambient air, and yet is relatively inert, making the molecule a viable target for absorption measurements in many high-temperature gas flows where it may be present naturally or can be added. Figure 1 shows the infrared absorption spectra of CO₂ from 1 to 5 μm in wavelength, plotted as line-strengths at 1,000 K. Absorption sensing technology in the 1.3–2.1 μm wavelength region is relatively mature due to the affordability and availability of optical components supporting the telecommunications industry. Therefore, many laser-based CO₂ absorption sensors have targeted the spectral combination bands near 1.5 μm ($2\nu_1 + 2\nu_2 + \nu_3$) [4, 5] and 2.0 μm ($\nu_1 + 2\nu_2 + \nu_3$) [6–8]. However, these absorption bands are relatively weak at increased temperatures ($T > 800\text{ K}$), and thus have limited range and applicability in high-temperature gas systems wherein CO₂ is not a major component. More recently, progress in diode laser technology has enabled spectroscopic access to the stronger vibrational band near 2.7 μm ($\nu_1 + \nu_3$), and

R. M. Spearrin (✉) · W. Ren · J. B. Jeffries · R. K. Hanson
High Temperature Gasdynamics Laboratory, Department of
Mechanical Engineering, Stanford University, Stanford,
CA 94305, USA
e-mail: spearrin@stanford.edu

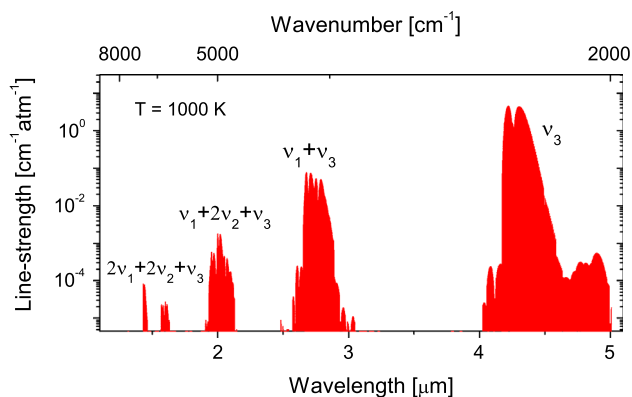


Fig. 1 Absorption line-strengths of CO₂ at 1,000 K (HITEMP [12])

researchers have developed temperature and species concentration diagnostics for shock tubes and pulse detonation engines by probing multiple CO₂ absorption transitions within this band [9–11]. The fundamental CO₂ vibrational band near 4.3 μm (ν_3) has approximately 70 and 3,000 times stronger absorption, respectively, than the combination bands at 2.7 and 2.0 μm. This fundamental band offers potential for much more sensitive detection than established CO₂ absorption sensors, though a lack of available room temperature tunable lasers at wavelengths of interest in this band has mitigated such advancement for highly quantitative spectroscopy at increased gas temperatures. Here, we have implemented an existing 2.7 μm diode laser with a newly developed tunable external cavity quantum cascade laser (ECQCL) that can access almost the entire ν_3 fundamental band of CO₂ (4.13–4.46 μm). The latter laser was utilized to advance spectroscopic strategies which enable improved sensitivity for temperature and CO₂ species concentration measurements in high-temperature gases.

In the present work, mid-infrared CO₂ sensing strategies were developed with an aim toward application in shock tube kinetics studies. The objectives of this research are twofold: (1) develop a highly sensitive (<100 ppm) CO₂ concentration diagnostic that is relatively insensitive to temperature changes common to reactive (pyrolysis/oxidation) experiments and (2) develop a sensitive temperature diagnostic based on mid-infrared CO₂ absorption which may be used for shock tube experiments with nascent or seeded CO₂. Two distinct strategies are presented to accomplish the aforementioned objectives, highlighting the flexibility of the broadly tunable external cavity QCL. The sensor is validated and refined at high temperatures (700–1,800 K) in shock-heated CO₂–argon mixtures and demonstrated in various pyrolysis and oxidation studies.

2 Theory

Absorption spectroscopy theory is briefly outlined to clarify notation and can be found more rigorously presented in other works [3, 13]. The Beer–Lambert law provides the fundamental physical relation governing narrow-band laser absorption spectroscopy. The equation relates the measurable incident (I_0) and transmitted (I_t) light intensities through a gas medium by

$$\left(\frac{I_t}{I_0}\right)_v = \exp(-\alpha_v), \quad (1)$$

where α_v represents the spectral absorbance at frequency ν (cm⁻¹). Spectral absorbance is related to gas properties, including temperature T (K) and species mole fraction x_{abs} , by

$$\alpha_v = -\ln\left(\frac{I_t}{I_0}\right)_v = Px_{\text{abs}}S_i(T)\phi(v)_iL, \quad (2)$$

where $S_i(T)$ (cm⁻² atm⁻¹) is the line-strength of a quantum transition i which varies only with temperature, $\phi(v)_i$ (cm) is the line-shape function and L (cm) is the path-length. It follows that gas temperature can be directly inferred from the ratio of spectral absorbance at two different wavelengths, as expressed in Eq. 3:

$$\left(\frac{\alpha_{\nu_1}}{\alpha_{\nu_2}}\right) = \frac{S_A(T)\phi(\nu_1)_A}{S_B(T)\phi(\nu_2)_B} = R(T). \quad (3)$$

The absorbance ratio simplifies to the ratio of the respective line-strengths and line-shape functions for each selected transition (A or B). With similar line-shape functions, temperature sensitivity of the absorbance ratio, $(dR/R)/(dT/T)$, is primarily driven by the line-strength ratio of the selected line-pair and can be approximated as

$$\left|\frac{dR/R}{dT/T}\right| \approx \left(\frac{hc}{k}\right) \frac{|E''_A - E''_B|}{T}, \quad (4)$$

where h (J-s) is Planck's constant, c (cm s⁻¹) is the speed of light, k (J/K) is Boltzmann's constant, and E'' (cm⁻¹) is the lower-state energy for the target absorption lines [14]. From Eq. 4, we note that the difference in lower-state energies between lines largely governs the temperature sensitivity for a two-line absorption technique and serves as a guide for line selection. Additional spectral parameters that affect the temperature dependence of the absorbance ratio include the difference in center wavelengths and line-shapes between selected lines.

The spectral line-shape functions were modeled here using the Voigt profile, which captures both collisional-broadening and temperature-broadening effects, characterized by a collisional width $\Delta\nu_c$ (cm⁻¹) and Doppler width $\Delta\nu_d$ (cm⁻¹), respectively. Though the Doppler width

scales simply with line-center wavelength and gas temperature, the collisional width depends on gas composition, with unique line-broadening effects for each molecular collision partner per

$$\Delta\nu_c = P \sum_j x_j 2\gamma_{j-\text{abs}}, \quad (5)$$

where P (atm) is total pressure and $\gamma_{j-\text{abs}}$ ($\text{cm}^{-1} \text{atm}^{-1}$) is the broadening coefficient between perturbing species j and the absorbing species. The temperature dependence of collisional-broadening is often modeled as a power law,

$$\gamma_j(T) = \gamma_j(T_0) \left(\frac{T_0}{T}\right)^n, \quad (6)$$

where n is the temperature dependence exponent.

Two-wavelength thermometry is a common spectroscopic method for quantifying gas temperature based on laser absorption of a single species [15–17]. With temperature either measured or known, species concentration can readily be determined per Eq. 2.

3 Line selection

Primary factors influencing line selection include the strength, isolation, and temperature sensitivity of accessible absorption transitions. The fundamental CO₂ asymmetric stretch (ν_3) band centered near 4.26 μm (2,350 cm^{-1}) consists of many strong rovibrational absorption lines. This ν_3 band is also generally well isolated from interfering absorption when among other combustion products and ambient species including water and carbon monoxide. However, due to the great strength of the fundamental band, ambient CO₂ (~ 400 ppm) absorbs significantly at typical path-lengths (~ 1 m) associated with benchtop optical setups, creating issues of self-interference. Figure 2 shows absorbance simulations of ambient (300 K) and high-temperature (1,000 K) CO₂ in the wavelength domain of the ν_3 band. As illustrated, even at a relatively short path-length (15 cm), ambient CO₂ can be optically thick for a large portion of the fundamental band, making utilization of this portion of the band difficult and impractical for many applications. At high temperatures, the Boltzmann distribution forces a more dispersed population of molecules among energy states, increasing the relative strength of absorption transitions associated with high lower-state energies. This makes the far wings of the fundamental band at frequencies below 2,300 cm^{-1} and above 2,380 cm^{-1} attractive wavelength regions for high-temperature applications [18].

The far wings of the fundamental ν_3 band contain many candidate lines with attractive characteristics for

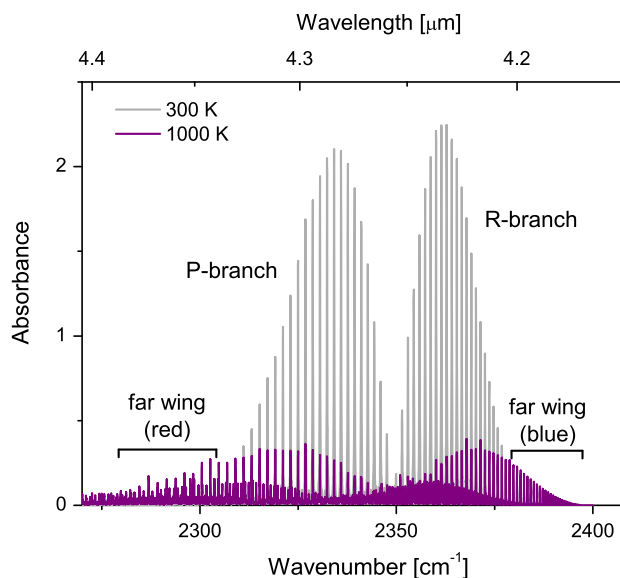


Fig. 2 Absorbance simulations for the CO₂ ν_3 band at $T = 300$ K and $T = 1,000$ K; $P = 1$ bar, $X_{\text{CO}_2} = 400$ ppm, $L = 15$ cm

quantitative laser absorption measurements in high-temperature environments. The HITEMP database [12] provides a comprehensive set of CO₂ line parameters including line-strengths, lower-state energies, and broadening coefficients which facilitate a detailed assessment and comparison of individual lines via simulated spectra at expected test conditions. An FTIR spectrometer (~ 0.1 cm^{-1} resolution) was also utilized in conjunction with a heated static cell to provide empirical validation for HITEMP simulations and assist in line selection. Details of the experimental setup involving the FTIR spectrometer and static cell can be found in a previous work [19]. Figure 3 shows measured CO₂ spectra in the far wings of the fundamental band and comparison with HITEMP simulations at increased temperature (700 K). The HITEMP simulation exhibits excellent agreement with the FTIR measurement, providing confidence in the tabulated line-strengths and air-broadening parameters. The figure also shows the interference from ambient CO₂ (400 ppm) at a 1-m path-length and room temperature. Comparison of the respective spectra in the far wings of the P-branch and R-branch reveals a substantial difference in relative line isolation between the two domains. Individual spectral lines in the P-branch have extensive interference with neighboring CO₂ lines at increased temperatures. This crowded P-branch spectrum is due to an abundance of active transitions comprising the fundamental hot bands, including $\nu(001 \rightarrow 002)$, $\nu(002 \rightarrow 003)$ and so on, where each progressive band center shifts to a lower wavenumber due to the decreasing spacing of vibrational energy levels. Thereby, the lines in the far wing of the R-branch are, in contrast, relatively well isolated, marking the spectral

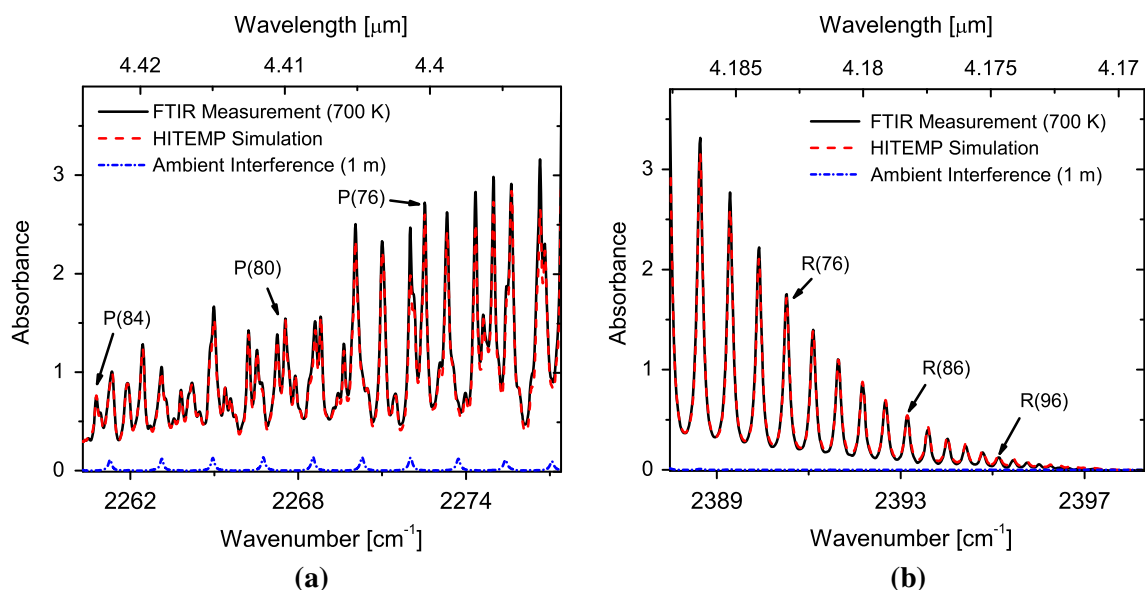


Fig. 3 Measured and simulated spectra in the far wings of the **a** P-branch and **b** R-branch of the CO₂ fundamental ν_3 band; $T = 700$ K, $P = 2$ bar, $L = 20.95$ cm, $X_{\text{CO}_2} = 1.5$ % in air; Simulated interference from ambient CO₂ (400 ppm) at $L = 1$ m, $T = 300$ K also shown

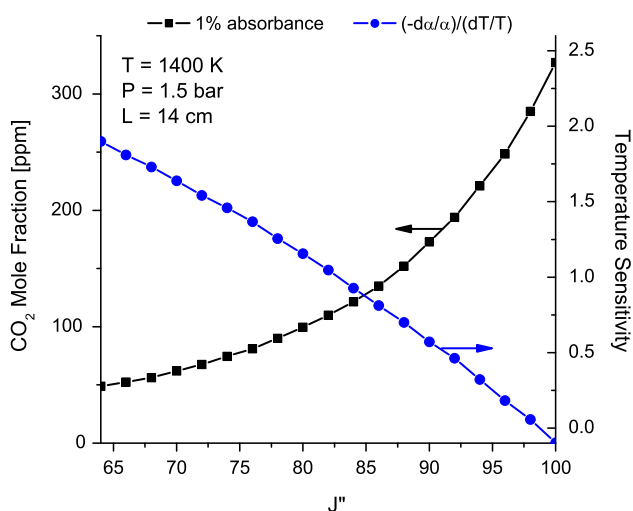


Fig. 4 Estimated detectability and temperature sensitivity of CO₂ using fixed-wavelength DA at line-center for candidate ν_3 R-branch lines; $T = 1,400$ K, $P = 1.5$ bar, $L = 14$ cm

domain around $2,381$ – $2,397$ cm^{-1} ideal for sensitive laser-based absorption sensing of CO₂ at increased temperatures. Selection of specific lines within the targeted 4.17 – 4.2 μm window of the ν_3 R-branch requires further consideration of the test conditions of interest and optical path-length of the shock tube.

As outlined, the first objective of this work is to provide highly sensitive detection (<100 ppm) of CO₂ for temperature-insensitive species concentration measurements in a shock tube. With test temperature known from the ideal

shock relations, a single-line measurement approach can be taken. Figure 4 shows the mole fraction of CO₂ for 1 % line-center absorbance (with Argon bath gas) at a typical test condition for each of 19 candidate lines in the R-branch labeled by their respective lower-state rotational quantum number (J''). Prior experience suggests that absorbance greater than 1 % provides sufficient signal for quantitative detection ($\text{SNR} > 10$) with an ECQCL based on a ~ 0.1 % absorbance detection limit [20]. Also plotted on the right axis is the temperature sensitivity of line-center absorbance for each transition. We see that temperature sensitivity decreases with J'' as the mole fraction for 1 % absorbance increases. To provide a requisite sub-100 ppm detectability while minimizing temperature sensitivity, the R(76) line near $2,390.52$ cm^{-1} is selected to compromise these opposing demands.

Sensitive two-line thermometry represents our second objective, and for these experiments CO₂ may be seeded in the shock tube test gas at modest concentrations (1–2 %) without meaningfully perturbing reaction chemistry. To achieve maximum temperature sensitivity, we primarily aim to select two lines with a large difference in lower-state energies ($\Delta E''$) as defined by Eq. 4. However, a large difference in lower-state energies is generally associated with a large difference in line-strengths (ΔS) and thus measured absorbance values when the two lines are selected from within the same band. A large difference in absorbance values is non-ideal due to limitations in dynamic range, bound by the optically thin and thick limits. The result is a tradeoff between temperature sensitivity and range when using conventional intra-band two-line

thermometry. In this work, we present a cross-band two-line CO₂ thermometry technique to both increase temperature sensitivity and expand the temperature range of utility

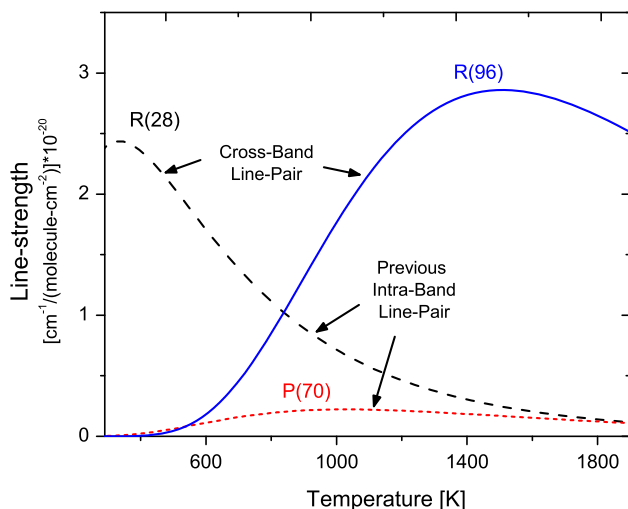


Fig. 5 Line-strengths versus temperature for transitions utilized in two-line CO₂ thermometry (past and present)

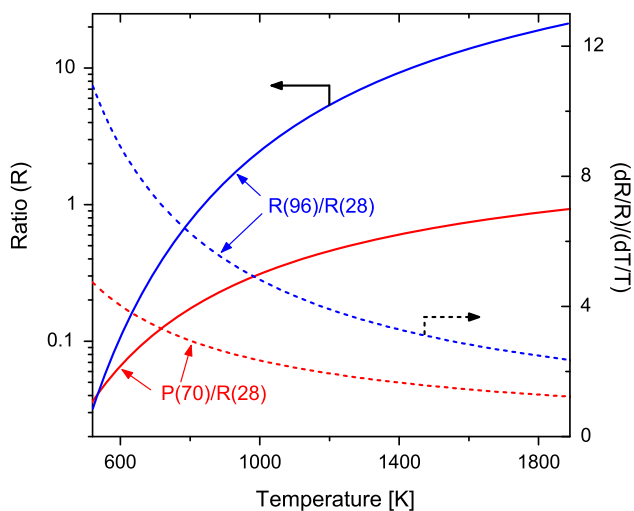


Fig. 6 Line-strength ratio and temperature sensitivity for cross-band line-pair compared to previous intra-band line-pair [9]

compared with previous intra-band sensors. We select two lines from different vibrational bands of CO₂ (ν_3 and $\nu_1 + \nu_3$), taking advantage of the sizable difference in band strengths to select a line-pair with a large $\Delta E''$ and a relatively small ΔS .

Relaxing the detectability requirement (100 ppm \rightarrow 1 %) for CO₂ thermometry allows us to select a line within the ν_3 R-branch that has a much higher E'' than the line selected to meet our first objective. Moreover, because low E'' transitions within the ν_3 band are very strong, selection of a line with a lower-state energy $<1,000$ cm⁻¹ leads to issues of self-interference with ambient CO₂ and a problematically large line-strength/absorbance ratio, $R(1,000 \text{ K}) > 25$, when paired to yield $\Delta E''$ greater than 2,000 cm⁻¹. In combination, these intra-band issues constrain both range and sensitivity for two-line thermometry. To address such difficulties, we look to the weaker $\nu_1 + \nu_3$ band near 2.7 μm to choose the low E'' line. The R(28) line near 3,633.08 cm⁻¹ is selected from the $\nu_1 + \nu_3$ band to serve as the low E'' line due to relative strength and isolation. This line has been utilized previously for intra-band thermometry at 2.7 μm in similar applications [9, 10, 21]. We pair this line with the R(96) transition near 2,395.13 cm⁻¹ in the ν_3 band to yield a $\Delta E''$ of 3,305 cm⁻¹. Figures 5 and 6 illustrate the expected temperature range and sensitivity of the new cross-band thermometry sensor, with comparison to the previous intra-band sensor at 2.7 μm [9]. Table 1 lists relevant spectral parameters associated with each line used in this work.

4 Sensor development

4.1 Light source selection

Two mid-infrared light sources are utilized for this sensor to access the three CO₂ lines of interest. Access to the R(76) and R(96) transitions near 4.2 μm is attained with a continuous-wave, single-mode ECQCL from Daylight Solutions. The quantum cascade laser is broadly tunable (2,240–2,420 cm⁻¹) over the CO₂ ν_3 band using a motorized grating (\sim Hz) and more precisely tuned over a small range by a piezoelectric driver (\sim 100 Hz). Figure 7 shows

Table 1 Spectroscopic line assignments and modeling parameters for the CO₂ lines of interest

Line	ν_0 (cm ⁻¹)	E'' (cm ⁻¹)	Band	$S(296 \text{ K})$ (cm ⁻² /atm)	$\gamma_{\text{Ar}}(1,000 \text{ K})$ (10 ⁻³ \times cm ⁻¹ /atm)	n_{Ar}	$\gamma_{\text{self}}(296 \text{ K})$ (10 ⁻³ \times cm ⁻¹ /atm)
R(76)	2,390.52	2,278	ν_3	10.1×10^{-3}	18.3 ± 0.6	0.60 ± 0.02	65
R(96)	2,395.14	3,622	ν_3	18.5×10^{-6}	16.4 ± 0.4	0.48 ± 0.02	63
R(28)	3,633.08	317	$\nu_1 + \nu_3$	59.5×10^{-2}	26.7 ± 0.7	0.51 ± 0.02	93

Parameters taken from HITEMP [12] except where measured ($\gamma_{\text{Ar}}, n_{\text{Ar}}$)

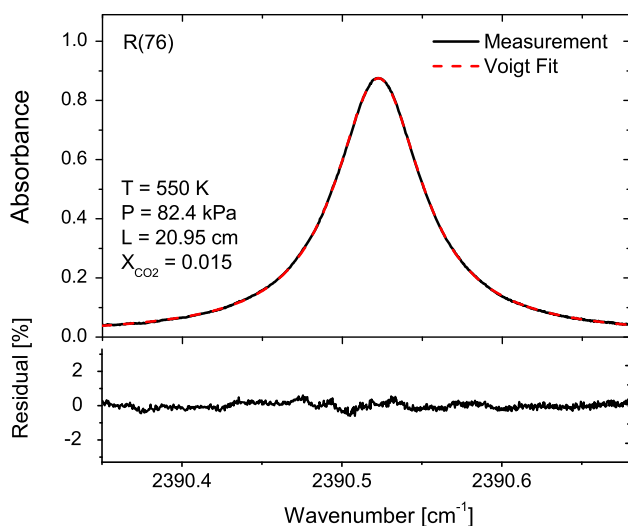


Fig. 7 Scanned-wavelength direct absorption measurement of the R(76) CO₂ transition using a Daylight Solutions ECQCL (100 Hz); $T = 550$ K, $P = 618$ torr, $L = 20.95$ cm, $X_{\text{CO}_2} = 0.015$ in air

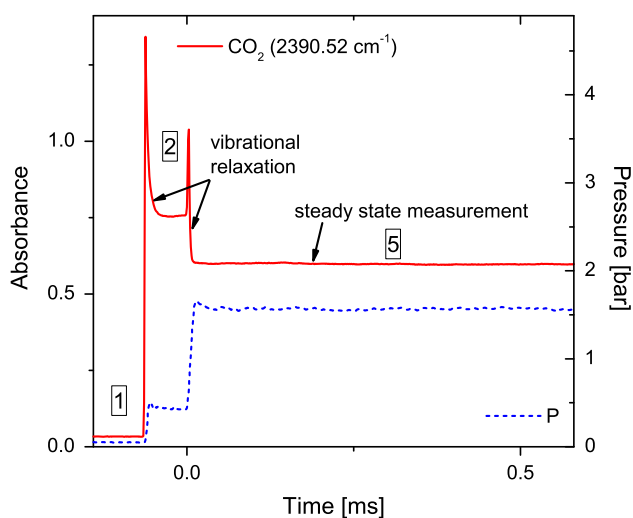


Fig. 8 Peak absorbance time-history for the R(76) line near $2,390.52$ cm⁻¹ during a non-reactive shock tube experiment of CO₂ dilute in argon; $X_{\text{CO}_2} = 0.005$, $L = 14.1$ cm, $T_5 = 1,540$ K

an example piezo scanned-wavelength measurement of the R(76) line using the ECQCL. Output power ranges from 30 to 100 mW depending on wavelength, with a typical power of 40 mW at 4.2 μm . The ECQC laser linewidth is ~ 5 MHz with a wavelength stability of ± 0.002 cm⁻¹ in a fixed-wavelength mode. The R(28) transition of the $\nu_1 + \nu_3$ band is probed with a DFB diode laser from Nanoplus centered near 2.75 μm with an output power of ~ 5 mW. The diode laser linewidth is ~ 3 MHz with wavelength stability of ± 0.001 cm⁻¹ and a tunability range of ± 3 cm⁻¹.

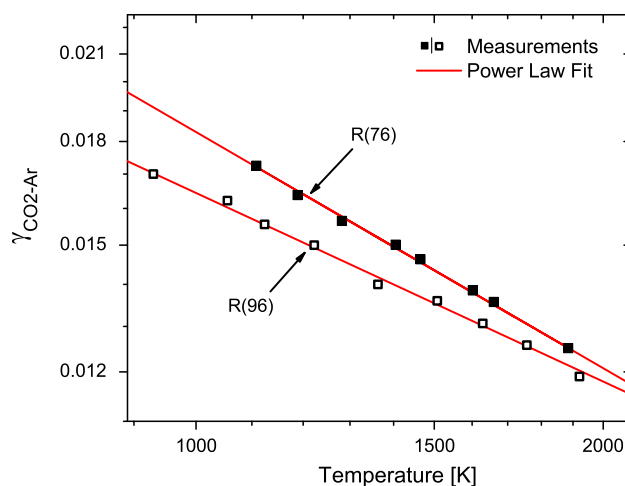


Fig. 9 Argon-broadening coefficients for the R(76) and R(96) CO₂ lines

4.2 Spectral modeling

Accurate fixed-wavelength direct absorption (fixed-DA) measurements require a comprehensive spectral model. The HITEMP database combined with the Voigt line-shape function has been demonstrated for very accurate modeling of the infrared CO₂ spectra in air, as shown in Fig. 3 and documented elsewhere [11, 22, 23]. However, shock tube kinetics studies are commonly carried out with argon as the bath gas, for which collisional-broadening and collisional-shifting parameters do not exist in the HITEMP database. For the R(28) line of the $\nu_1 + \nu_3$ band, these parameters have been measured by previous researchers [9]. To account for argon-broadening and shifting parameters of the R(76) and R(96) lines of the ν_3 band, static cell and non-reactive shock tube measurements were made of CO₂ dilute in argon in order to adjust our spectral model. First, measurements in a heated static cell confirmed that pressure shift in argon is small and negligibly different than pressure shift in air over the conditions of interest. Second, in addition to the relatively low-resolution FTIR spectrometer measurements, the ECQCL was used to validate HITEMP line-strength values for spectral lines near 4.2 μm using a scanned-wavelength (100 Hz) direct absorption method. In these experiments, a Voigt line-shape function was fit to the experimental data, as shown in Fig. 7, from which an integrated absorbance area (A_i) could be extracted and related directly to line-strength by: $A_i = P x_{\text{abs}} S_i(T) L$. Measured line-strength values agreed with HITEMP tabulated values within measurement uncertainty ($< 2\%$). Using the Voigt function, the only remaining parameter necessary to fully characterize the spectral line-shape is the argon-broadening coefficient.

Here, we inferred argon-broadening coefficients at temperatures of interest (700–1,800 K) by making fixed-wavelength measurements at the absorbance peak of each line during non-reactive shocks of CO₂ dilute in argon. Experiments in the shock tube provide well-defined environments for short time periods (~ms) at temperatures not attainable in a static cell (>1,000 K). Figure 8 shows an example time-history of a non-reactive shock tube experiment assessing the R(76) line near 2,390.52 cm⁻¹ at 1,540 K. Based on the measured pressure and dilute nature of the gas mixture, the broadening coefficient at a given temperature is effectively solved by Eq. 5, where peak absorbance and collisional width are uniquely coupled in the spectral model. Such experiments are critical for understanding the temperature dependence of collisional-broadening, which is not well defined by Eq. 6 over a large temperature range, and thus cannot be reliably inferred from low-temperature measurements alone [24, 25]. Measured broadening coefficients for the R(76) and R(96) lines of the ν_3 band are shown in Fig. 9 over a range of temperatures (800–1,900 K) and each fit with a respective power law function. These measurements are consistent with other CO₂-Ar broadening measurements in an FTIR (550–800 K) by Thibault et al. [26]. Caution should be exercised when extending the respective power law functions based on this data to a wider range of temperature. Collisional-broadening parameters for all three lines used in this work, as well as other relevant spectroscopic modeling parameters associated with the CO₂ lines, are given in Table 1. Further detail on the experimental setup is discussed in the subsequent section.

4.3 Optical setup

Figure 10 shows a representative optical setup for the current shock tube experiments. The lasers were used both

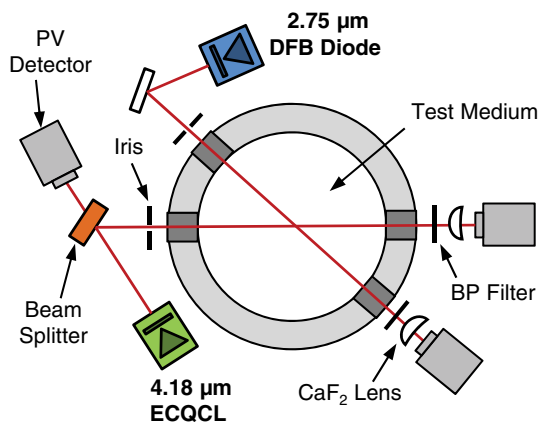


Fig. 10 Optical setup for shock tube experiments

independently (for spectral validation and ultra-sensitive species detection) and in combination as shown (for thermometry). The shock tube has a 14.13-cm internal path-length and barium fluoride windows located approximately 2 cm from the end wall. The incident beam from the quantum cascade laser (4.2 μm) is split with an anti-reflection coated calcium fluoride beam splitter to provide a reference signal for common-mode intensity noise rejection. The diode laser (2.7 μm) exhibits intensity noise of <0.2 % of absolute signal, and the ECQCL can achieve similar intensity stability after common-mode rejection. The beams from both lasers (QCL and diode) are collimated and spatially conditioned with an iris to be ~2 mm in diameter prior to entering the test section at co-planar angles. Each laser beam is spectrally filtered with a band-pass filter (~60 nm) after passing through the test section and focused onto a photovoltaic detector by a calcium fluoride plano-convex lens (20 mm f.l.). The photovoltaic detectors (Vigo PVI-X) are aligned collinear with the beam path and are thermo-electrically cooled, having a 2-mm detection area and 10-MHz bandwidth. Data from the detectors are collected at a sample rate of 1 MHz. Between tests, a wavelength meter (Bristol 621B) is used to verify that each laser is centered at line-center. More detailed information on the shock tube utilized for this work can be found in previous writings [27, 28].

5 Demonstration and validation

5.1 Sensitive species concentration measurements

The first objective of this work was to provide the ability for ultra-sensitive (<100 ppm) species concentration measurements of CO₂ with minimal temperature dependence. This strategy is targeted for utilization in multi-species measurement campaigns in shock tubes to inform and improve the modeling of chemical kinetic mechanisms. In previous research, limited resolution in CO₂ concentration measurements (~300 ppm) based on absorption at 2.7 μm required the utilization of greater initial fuel concentrations (2–3 %) than desired [29], which leads to larger changes in temperature during the experiment that can meaningfully alter the kinetic interpretation. Additionally, to achieve the aforementioned resolution in the 2.7 μm band, the relatively strong R(28) line was used, which has a larger temperature sensitivity than lines at higher rotational quantum numbers. To improve on these aspects, we probed the R(76) transition near 4.2 μm to achieve greater absolute sensitivity and lower temperature dependence as discussed in Sect. 3. Figure 11 shows example species time-histories during oxidation of methyl butyrate (MB) at several temperatures to exhibit the high-fidelity data producible with the new sensor. The sensor

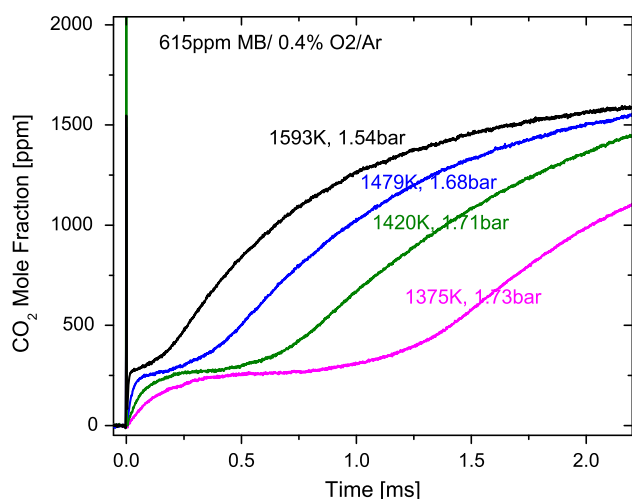


Fig. 11 Measured CO_2 species time-histories during methyl butyrate oxidation ($\phi \approx 1$)

demonstrates the ability to resolve complex kinetic mechanisms on multiple time scales in a self-consistent manner at fuel concentrations more than ten times lower than previous experiments. Figure 12 highlights the improved detection limit of the new sensing strategy and the ability to resolve kinetic rate information at early times, critical for anchoring chemical mechanisms. Based on an observed signal-to-noise ratio (SNR) of ~ 10 at 50 ppm, the detection limit of the current sensor is approximately 5 ppm with 1 MHz bandwidth at typical shock tube conditions. Results of the first kinetic studies utilizing this new sensor were presented in a separate paper by the current authors [30].

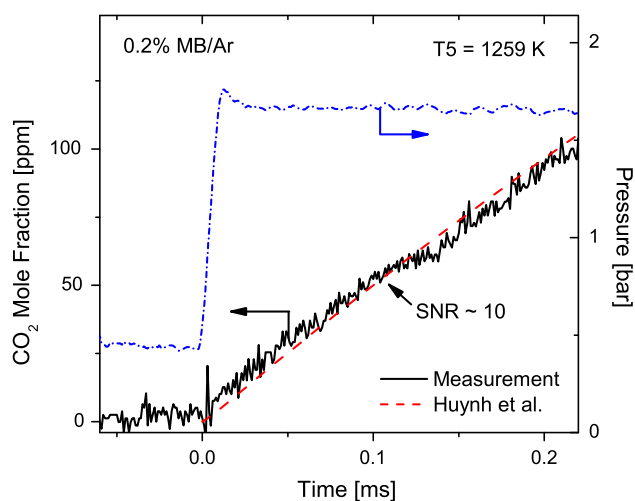


Fig. 12 Pressure and CO_2 species time-histories during methyl butyrate pyrolysis at 1,259 K with comparison to the kinetic model of Huynh et al. [31]

5.2 Cross-band thermometry

The sensitive cross-band thermometry technique, utilizing the R(96) and R(28) lines, was validated in the same shock tube as discussed previously. Non-reactive CO_2 -Ar shocks were performed over a range of temperatures (600–1,800 K) and pressures (1.2–2.5 bar) to evaluate the accuracy of the spectral model and the precision of the fixed-wavelength sensor. An example time-history of the shock tube validation is shown in Fig. 13, wherein the strong inverse temperature dependence can be observed between the two wavelengths as the experiment proceeds in time, and increases in temperature. This strong inverse dependence yields the high level of temperature sensitivity in the ratio of absorbances. With similar line-strengths, the concentration of CO_2 in the bath gas can be readily tailored to optimize the absorbance magnitudes between the optically thin and thick limits ($\alpha \approx 0.1$ –1.5) over a wide range of temperatures. As seen in the figure, both wavelengths provide favorable absorbance levels with 2 % CO_2 seeded in the bath gas.

The ratio of absorbances was then converted to temperature, as depicted in Fig. 14, based on the respective spectral models for each wavelength, using the measured pressure and known mole fraction as inputs. For each shock, temperature was also calculated from the measured incident shock velocity using the ideal shock relations and known initial conditions in the shock tube. Typical uncertainty in temperature using this calculated method is approximately 0.6 % for non-reactive shocks and treated as the known temperature here [32]. The known temperatures (pink) for region 2 (between incident and reflected shock) and region 5 (after reflected shock) are shown overlaid with

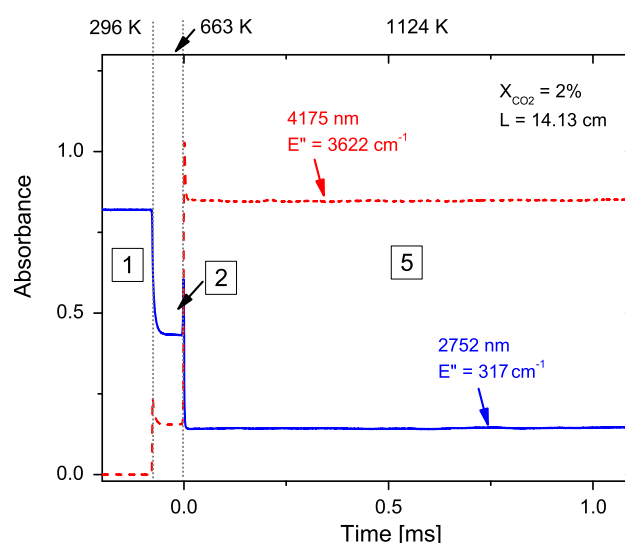


Fig. 13 Example peak absorbance time-histories of the R(96) and R(28) lines in a non-reactive shock tube experiment

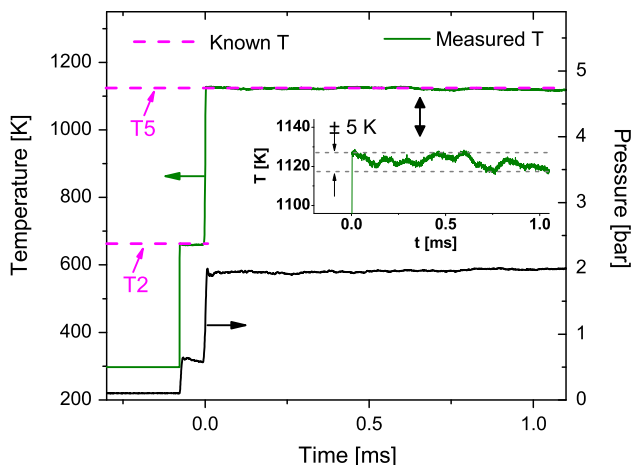


Fig. 14 Measured temperature based on cross-band thermometry for a non-reactive CO₂-Ar shock (same as Fig. 13) with comparison to calculations from the ideal shock relations

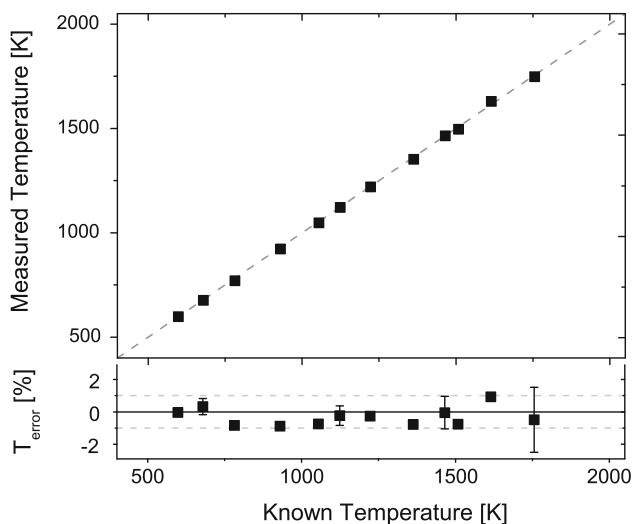


Fig. 15 Comparison of cross-band thermometry with known temperature in the shock tube

the measured temperature from cross-band CO₂ thermometry, with excellent agreement displayed between the two methods. Looking more closely at the measured temperature behind the reflected shock reveals the precision that can be achieved using the cross-band technique (± 5 K or <0.5 %) over the test time (~ 1 ms) of the non-reactive shock. Figure 15 provides an assessment of the accuracy of the cross-band technique, comparing the measured temperatures to the known temperatures from the ideal shock relations. Over the full range of conditions, the measured temperature agreed with the known temperature within 1 %, and the standard error was ~ 0.5 %. Precision decreased with temperature such that noise in the

temperature measurement reached ± 2 % at the high end of the temperature range compared with a typical 0.5 % as illustrated in Fig. 14.

6 Summary

Accurate and precise determination of temperature and species concentration is important to the assessment of reacting gas systems. In this work, we developed a highly sensitive laser-based absorption diagnostic that probes the infrared spectra of CO₂ to measure gas temperature and CO₂ concentration at time scales (μ s) and temperatures (600–1,800 K) relevant for shock tube kinetics studies. An ECQCL was utilized to exploit the far R-branch wing of the fundamental ν_3 band of CO₂ near 4.2 μ m, which is well isolated from potential interfering absorption. The R(76) line was selected for sensitive (<100 ppm) species detection with relatively weak temperature dependence. Oxidation and pyrolysis experiments were performed on various methyl esters, wherein the sensor exhibited a detection limit of better than 5 ppm at conditions of interest for combustion kinetics. This mid-infrared (4.2 μ m) CO₂ concentration sensing represents an improvement of greater than 50 times the sensitivity achieved previously near 2.7 μ m. A cross-band two-line thermometry technique was also established using the R(96) line of the ν_3 fundamental band and the R(28) line of the $\nu_1 + \nu_3$ combination band. The cross-band spectroscopic approach facilitates high-temperature sensitivity ($\Delta E'' > 3,000$ cm⁻¹) with similar ranges of absorbance between the two lines, which is desirable in order to maximize the useful range of the sensor. Non-reactive CO₂-in-argon shocks were carried out to validate the accuracy (~ 0.5 %), precision (0.2–2 %), and range (600–1,800 K) of the cross-band thermometry technique. Compared with previous intra-band fixed-DA thermometry methods, this cross-band method offers more than twice the sensitivity along with expanded useful range to higher temperatures.

7 Potential sensor improvements

While the current sensor substantially improves upon prior CO₂ absorption sensing techniques, future work is recommended to further optimize the sensor and expand its applicability. Normalized wavelength modulation techniques (WMS- $n/f/mf$) can be employed to desensitize measurements to non-absorption light intensity fluctuations such as emission, beam steering, and vibrations that may limit precision, especially at the high end of the temperature range. WMS methods can also desensitize measurements to spectrally broad

interfering absorption, which may be present with various fuels. Additionally, the optical engineering of the current sensor may be improved to create a more field-deployable diagnostic. Specifically, the two beams for thermometry may be combined onto a single optical path, using a beam splitter or bifurcated optical fiber, to minimize the optical footprint of the sensor and mitigate the influence of spatial non-uniformities in the test gas, which are more pronounced in engine applications. From a spectroscopic standpoint, the ECQCL may also be utilized to probe any of the thirty well-isolated CO₂ transitions in the ν_3 R-branch between 2,381 and 2,397 cm⁻¹, which may be desirable for certain applications with slightly different test conditions, detection requirements, and path-lengths. Here, we have demonstrated two distinct applications, for which the R(76) and R(96) lines were used, but the current diagnostic offers additional flexibility in line selection, and can be optimized for a broad range of high-temperature applications.

Acknowledgments All experiments discussed herein were performed at the High Temperature Gasdynamics Laboratory at Stanford University. Support for these experiments was provided by the Air Force Office of Scientific Research (AFOSR) with Chiping Li as contract monitor. We would also like to acknowledge Andy Tulgestke and Luke Zaczek for their support in operating the shock tube for sensor demonstration.

References

1. H. Teichert, T. Fernholz, V. Ebert, Simultaneous in situ measurement of CO, H₂O, and gas temperatures in a full-sized coal-fired power plant by near-infrared diode lasers. *Appl. Opt.* **42**, 2043 (2003)
2. J. Hodgkinson, R.P. Tatam, Optical gas sensing: a review. *Meas. Sci. Technol.* **24**, 012004 (2013)
3. R.K. Hanson, Applications of quantitative laser sensors to kinetics, propulsion and practical energy systems. *Proc. Combust. Inst.* **33**, 1–40 (2011)
4. R.M. Mihalcea, D.S. Baer, R.K. Hanson, A diode-laser absorption sensor system for combustion emission measurements. *Meas. Sci. Technol.* **9**, 327–338 (1998)
5. D.M. Sonnenfroh, M.G. Allen, Observation of CO and CO₂ absorption near 1.57 μm with an external-cavity diode laser. *Appl. Opt.* **36**, 3298 (1997)
6. R.M. Mihalcea, D.S. Baer, R.K. Hanson, Diode-laser absorption measurements of CO₂ near 2.0 μm at elevated temperatures. *Appl. Opt.* **37**, 8341 (1998)
7. G.B. Rieker, J.B. Jeffries, R.K. Hanson, Measurements of high-pressure CO₂ absorption near 2.0 μm and implications on tunable diode laser sensor design. *Appl. Phys. B* **94**, 51–63 (2008)
8. M.E. Webber, R. Claps, F.V. Englich, F.K. Tittel, J.B. Jeffries, R.K. Hanson, Measurements of NH₃ and CO₂ with distributed-feedback diode lasers near 2.0 μm in bioreactor vent gases. *Appl. Opt.* **40**, 4395 (2001)
9. A. Farooq, J.B. Jeffries, R.K. Hanson, CO₂ concentration and temperature sensor for combustion gases using diode-laser absorption near 2.7 μm . *Appl. Phys. B* **90**, 619–628 (2008)
10. W. Ren, J.B. Jeffries, R.K. Hanson, Temperature sensing in shock-heated evaporating aerosol using wavelength-modulation absorption spectroscopy of CO₂ near 2.7 μm . *Meas. Sci. Technol.* **21**, 105603 (2010)
11. R.M. Spearrin, C.S. Goldenstein, J.B. Jeffries, R.K. Hanson, Fiber-coupled 2.7 μm laser absorption sensor for CO₂ in harsh combustion environments. *Meas. Sci. Technol.* **24**, 055107 (2013)
12. L.S. Rothman, I.E. Gordon, R.J. Barber, H. Dothe, R.R. Gamache, A. Goldman, V.I. Perevalov, S.A. Tashkun, J. Tennyson, HITEMP, the high-temperature molecular spectroscopic database. *J. Quant. Spectrosc. Radiat. Transf.* **111**, 2139–2150 (2010)
13. U. Platt, J. Stutz, *Differential Optical Absorption Spectroscopy: Principles and Applications* (Springer, Berlin, 2008), p. 597
14. X. Zhou, X. Liu, J.B. Jeffries, R.K. Hanson, Development of a sensor for temperature and water concentration in combustion gases using a single tunable diode laser. *Meas. Sci. Technol.* **14**, 1459–1468 (2003)
15. J. Vanderover, W. Wang, M.A. Oehlschlaeger, A carbon monoxide and thermometry sensor based on mid-IR quantum-cascade laser wavelength-modulation absorption spectroscopy. *Appl. Phys. B* **103**, 959–966 (2011)
16. I. A. Schultz, C. S. Goldenstein, J. B. Jeffries, R. K. Hanson, TDL absorption sensor for in situ determination of combustion progress in scramjet ground testing, in *28th Aerodynamic Measurement Technology, Ground Testing, and Flight Testing Conference* (2012)
17. S.H. Pyun, J.M. Porter, J.B. Jeffries, R.K. Hanson, J.C. Montoya, M.G. Allen, K.R. Sholes, Two-color-absorption sensor for time-resolved measurements of gasoline concentration and temperature. *Appl. Opt.* **48**, 6492–6500 (2009)
18. M.Y. Perrin, J.M. Hartmann, Temperature-dependent measurements and modeling of absorption by CO₂-N₂ mixtures in the far line-wings of the 4.3 μm CO₂ band. *J. Quant. Spectrosc. Radiat. Transf.* **42**, 311–317 (1989)
19. A.E. Klingbeil, J.B. Jeffries, R.K. Hanson, Temperature-dependent mid-IR absorption spectra of gaseous hydrocarbons. *J. Quant. Spectrosc. Radiat. Transf.* **107**, 407–420 (2007)
20. X. Chao, J.B. Jeffries, R.K. Hanson, In situ absorption sensor for NO in combustion gases with a 5.2 μm quantum-cascade laser. *Proc. Combust. Inst.* **33**, 725–733 (2011)
21. A. Farooq, J.B. Jeffries, R.K. Hanson, Sensitive detection of temperature behind reflected shock waves using wavelength modulation spectroscopy of CO₂ near 2.7 μm . *Appl. Phys. B* **96**, 161–173 (2009)
22. A. Farooq, J.B. Jeffries, R.K. Hanson, Measurements of CO₂ concentration and temperature at high pressures using 1f-normalized wavelength modulation spectroscopy with second harmonic detection near 2.7 micron. *Appl. Opt.* **48**, 6740–6753 (2009)
23. R. Sur, K. Sun, J. B. Jeffries, R. K. Hanson, Multi-species laser absorption sensors for in situ monitoring of syngas composition. *Appl. Phys. B* (2013). doi:10.1007/s00340-013-5567-2
24. R.T. Pack, Pressure broadening of the dipole and Raman lines of CO₂ by He and Ar. Temperature dependence. *J. Chem. Phys.* **70**, 3424 (1979)
25. L. Rosenmann, J.M. Hartmann, M.Y. Perrin, J. Taine, Accurate calculated tabulations of IR and Raman CO₂ line broadening by CO₂, H₂O, N₂, O₂ in the 300–2,400-K temperature range. *Appl. Opt.* **27**, 3902–3906 (1988)
26. F. Thibault, B. Calil, J. Buldyreva, M. Chrysos, J.-M. Hartmann, J.-P. Bouanich, Experimental and theoretical CO₂-Ar pressure-broadening cross sections and their temperature dependence. *Phys. Chem. Chem. Phys.* **3**, 3924–3933 (2001)
27. M.A. Oehlschlaeger, D.F. Davidson, R.K. Hanson, High-temperature thermal decomposition of isobutane and n-butane behind shock waves. *J. Phys. Chem. A* **108**, 4247–4253 (2004)
28. I. Stranic, D.P. Chase, J.T. Harmon, S. Yang, D.F. Davidson, R.K. Hanson, Shock tube measurements of ignition delay times for the butanol isomers. *Combust. Flame* **159**, 516–527 (2012)

29. A. Farooq, D.F. Davidson, R.K. Hanson, L.K. Huynh, A. Violi, An experimental and computational study of methyl ester decomposition pathways using shock tubes. *Proc. Combust. Inst.* **32**, 247–253 (2009)
30. W. Ren, R.M. Spearrin, D.F. Davidson, R.K. Hanson, Thermal decomposition of C3-C5 ethyl esters: CO, H₂O and CO₂ time-histories behind reflected shock waves, in *The 8th National Combustion Mtg* (2013), p. 11
31. L.K. Huynh, K.C. Lin, A. Violi, Kinetic modeling of methyl butanoate in shock tube. *J. Phys. Chem. A* **112**, 13470–13480 (2008)
32. I. Stranic, D.F. Davidson, R.K. Hanson, Shock tube measurements of the rate constant for the reaction cyclohexene → ethylene + 1,3-butadiene. *Chem. Phys. Lett.* **584**, 18–23 (2013)